RSC Advances

PAPER

View Article Online
View Journal | View Issue

Cite this: *RSC Adv.*, 2021, **11**, 21885

Lewis acid Ni/Al-MCM-41 catalysts for H_2-free deoxygenation of *Reutealis trisperma* oil to biofuels†

Reva Edra Nugraha, [ab] Didik Prasetyoko, *[a] Hasliza Bahruji, [c] Suprapto Suprapto, [a] Nurul Asikin-Mijan, [d] Titie Prapti Oetami, [e] Aishah Abdul Jalil, [fg] Dai-Viet N. Vo [hi] and Yun Hin Taufiq-Yap [jk]

The activity of mesoporous Al-MCM-41 for deoxygenation of *Reutealis trisperma* oil (RTO) was enhanced *via* modification with NiO nanoparticles. Deoxygenation at atmospheric pressure and under H_2 free conditions required acid catalysts to ensure the removal of the oxygenated fragments in triglycerides to form liquid hydrocarbons. NiO at different weight loadings was impregnated onto Al-MCM-41 and the changes of Lewis/Brønsted acidity and mesoporosity of the catalysts were investigated. The activity of Al-MCM-41 was enhanced when impregnated with NiO due to the increase of Lewis acidity originating from NiO nanoparticles and the mesoporosity of Al-MCM-41. Increasing the NiO loading enhanced the Lewis acidity but not Brønsted acidity, leading to a higher conversion towards liquid hydrocarbon yield. Impregnation with 10% of NiO on Al-MCM-41 increased the conversion of RTO to hydrocarbons *via* the deoxygenation pathway and reduced the products from cracking reaction, consequently enhancing the green diesel (C11–C18) hydrocarbon products.

Received 22nd April 2021
Accepted 10th June 2021

DOI: 10.1039/d1ra03145g

rsc.li/rsc-advances

Introduction

According to the International Energy Agency (IEA), 81.7% of the energy consumption in the world is derived from fossil fuel, and the demand was predicted to increase by 53% at the end of 2030.[1,2] The depletion of fossil fuel and the fluctuation of oil price have opened up windows of opportunity for researchers to develop energy from renewable resources.[3,4] Solar, wind, geothermal, hydrogen power, fuel cells and biofuel have been investigated as alternative energy sources or energy carriers, and each technology has the potential to fulfil the demand depending on the geography and the climate of the region.[5,6] In tropical countries, the development of biofuel has gained increasing popularity due to the availability of biomass as carbon feedstock.[7,8] Non-edible oil such as *Jatropha curcas* oil,[9–11] waste cooking oil,[12,13] palm fatty acid distillate (PFAD),[14,15] macauba oil,[16] calophyllum oil,[17] karanja oil[18] and *Reutealis trisperma* oil (RTO) have been investigated as carbon feedstocks for bio-fuel production. *Reutealis trisperma* is largely grown in Asian countries such as Philippine, Indonesia, Malaysia, India and China.[19] The tree can grow up to 10–15 m in height. Meanwhile, the seeds contain up to 52% of triglycerides.[20] RTO has been investigated as a feedstock for biodiesel production *via* ester/transesterification reaction.[19–23] However, biodiesel has low thermal stability and low calorific value due to its high oxygen content.[24–26] Conversion of triglycerides into hydrocarbon *via* deoxygenation reaction is another alternative route to enhance the calorific value and the thermal stability while reducing the corrosiveness and the viscosity of biofuel.[27]

Deoxygenation can be carried out *via* hydrodeoxygenation (HDO) or decarbonylation and decarboxylation (deCOx) reactions[7] as given in Table 1. In HDO, the reaction was conducted in hydrogen, at high pressure (20–200 bar) and temperature (200–450 °C) in order to reduce the oxygenated fragments.[16,27,28] However

[a]*Department of Chemistry, Faculty of Science and Data Analytics, Institut Teknologi Sepuluh Nopember, Keputih, Sukolilo, Surabaya 60111, Indonesia. E-mail: didikp@chem.its.ac.id; didik.prasetyoko@gmail.com*

[b]*Department of Chemical Engineering, Faculty of Engineering, Universitas Pembangunan Nasional "Veteran" Jawa Timur, Surabaya, East Java, 60294, Indonesia*

[c]*Centre of Advanced Material and Energy Sciences, Universiti Brunei Darussalam, Jalan Tungku Link, BE 1410, Brunei*

[d]*Department of Chemical Sciences, Faculty of Science and Technology, Universiti Kebangsaan Malaysia, 43600 UKM Bangi, Selangor, Malaysia*

[e]*Agrindo Company, Raya Driyorejo Km. 19, Gresik, East Java, Indonesia*

[f]*School of Chemical and Energy Engineering, Faculty of Engineering, Universiti Teknologi Malaysia, Skudai, Johor Bahru, Johor, 81310, Malaysia*

[g]*Centre of Hydrogen Energy, Institute of Future Energy, Universiti Teknologi Malaysia, Skudai, Johor Bahru, Johor, 81310, Malaysia*

[h]*Institute of Environmental Sciences, Nguyen Tat Thanh University, Ho Chi Minh City 755414, Vietnam*

[i]*College of Medical and Health Science, Asia University, Taichung, Taiwan*

[j]*Department of Chemistry, Faculty of Science, Universiti Putra Malaysia, UPM Serdang, Selangor, 43400, Malaysia*

[k]*Chancellery Office, Universiti Malaysia Sabah, Kota Kinabalu, Sabah, 88400, Malaysia*

† Electronic supplementary information (ESI) available. See DOI: 10.1039/d1ra03145g

Table 1 Reported studies on deoxygenation reaction *via* hydrodeoxygenation (HDO) or decarbonylation and decarboxylation (deCOx) on various biomass and catalysts

Catalyst	Reactant	Catalyst amount (%)	Reaction conditions	Conversion (%)	Diesel selectivity (%)	Ref.
TiO_2	Triolein	5	H_2, 380 °C, 8 h, semi-batch reactor	76.0	60	32
Al_2O_3–TiO_2	Triolein	5	Vacuum, 10 mbar, 380 °C, 1 h, semi-batch reactor	76.86	79.38	36
5%NiO/Al-SBA	PFAD[a]	5	N_2, 350 °C, 2 h, semi-batch reactor	—	91	14
Ni–Co/SBA-15	PFAD[a]	10	N_2, 350 °C, 3 h, semi-batch reactor	—	88.1	37
1%Pd/P25-TiO_2	Beef fat oil	—	H_2, 325 °C, 4 h dodecane as solvent, flow fixed-bed	96.9	66.2	38
Ni–Mg/MWCNT	Chicken fat oil	3	N_2, 350 °C, 2 h, semi-batch reactor	—	87	26
Ni–Ag/AC	JCO[b]	5	N_2, 350 °C, 2 h, semi-batch reactor	—	83	11
Co/EAC	Macauba oil	10	H_2, 350 °C, 2 h, dodecane as solvent, batch	97.59	96.7	16
10%Ni/Al-MCM-41	RTO[c]	3	N_2, 350 °C, 4 h, semi-batch reactor	68.53	98.6	*Present work*

[a] PFAD = palm fatty acid distillate. [b] JCO = *Jatropha curcas* oil. [c] RTO = *Reutealis trisperma* oil.

unlike HDO, deCOx was carried out in the absence of H_2. The oxygen was removed *via* elimination of carbonyl fragments as CO or CO_2, producing hydrocarbon with one atom carbon shorter than the parent structures.[29] Therefore, the presence of acid catalyst is crucial to enhance C–C bond dissociation. Apart from acidity, mesoporosity also plays an important role in enhancing the diffusion of triglycerides molecule and controlling the product selectivity of hydrocarbon. Mesoporous materials such as SBA-15,[14] Al-MCM-41,[30] mesoporous silica,[31] mesoporous TiO_2,[32] SiO_2–Al_2O_3 (ref. 33) and hierarchical zeolite[34] have been extensively investigated to improve the mass transfer. We have previously reported that mesoporous Al-MCM-41 enhanced the conversion of *Jatropha curcas* oil towards the long-chain (C11–C18) green diesel hydrocarbons when compared to mesoporous ZSM-5 due to the presence of highly ordered hexagonal mesopores.[35] Since the synthesis of Al-MCM-41 was carried out at high Si/Al ratio in order to ensure mesoporosity, the catalysts has low acidity which consequently results in poor conversion of oil.[35] This research aimed to increase the activity of mesoporous Al-MCM-41 for deoxygenation of *Reutealis trisperma* oil by increasing the acidity using NiO nanoparticles. NiO loading was varied to obtain the optimum acidity while minimizing the detrimental effect towards the mesoporosity of Al-MCM-41. The amount of Lewis and Brønsted acidity were determined using pyridine-FTIR analysis, meanwhile the structural changes of Al-MCM-41 were analysed using XRD, N_2 adsorption–desorption, SEM and TEM analysis. The conversion of oil and the hydrocarbon yield were correlated with the acidity and the structural properties of the catalysts. The results provided further understanding on the roles of Lewis/Brønsted acid sites and mesoporosity of Ni/Al-MCM-41 toward the conversion and the distribution of hydrocarbon produced from deoxygenation reaction.

Experimental

Materials

Kaolin $Al_4(Si_4O_{10})(OH)_8$ as silica and alumina sources was collected from Bangka Belitung, Indonesia. The kaolin consisted of 57% SiO_2 and 22% Al_2O_3. The *Reutealis trisperma* oil (RTO) as feedstock was acquired from PT. Agrindo Company, Gresik, Indonesia. NaOH (>99%) was purchased from Merck, Germany. LUDOX® HS-40 colloidal silica (30% Si in water) and nickel(II) nitrate hexahydrate (99%) was purchased from Sigma Aldrich, Germany. *N*-Cetyl-*N*,*N*,*N*-trimethylammonium bromide (CTABr, $C_{19}H_{42}BrN$, 99%) was purchased from Applichem. All materials used in this work were analytical grade.

Synthesis Al-MCM-41 support

Al-MCM-41 was prepared using 10 Na_2O:100 SiO_2:2 Al_2O_3:1800 H_2O of molar composition.[35] NaOH (1.60 g) was dissolved in demineralized water with continuous stirring for 30 min. Kaolin (1.85 g) was added gradually followed with Ludox (37.09 g) under vigorous stirring. Demineralized water was added into the mixture and stirred for 8 h. The resulting gel was aged for 6 h at 70 °C and transferred into autoclave with Teflon liner at 330 mL capacity and heated at 80 °C for 12 h. The autoclave was cooled immediately to stop the crystallization process. CTABr (18.93 g) as mesopore template (SiO_2/CTABr = 3.85) was added slowly into the mixture and stirred for 1 hour. The crystallization was continued for another 24 h at 150 °C. The solid product was filtered and washed using distilled water until the pH of the supernatant was neutral. The product was oven dried at 60 °C for 24 h and calcined at 550 °C (2 °C min^{-1}) under N_2 for 1 h then replaced with air for another 6 h. The yield of Al-MCM-41 powder obtained from the synthesis was 18 g.

Synthesis Ni/Al-MCM-41

Ni/Al-MCM-41 catalysts were prepared by impregnation method using aqueous $Ni(NO_3)_2$ solutions with Ni content of 5, 10, 15 and 20%. All percentages used in this experiment were in weight percent. The calculated amount of $Ni(NO_3)_2 \cdot 6H_2O$ was dissolved in demineralized water (10 mL) under continuous stirring. 1 g of Al-MCM-41 powder was added into the solution and stirred at ambient temperature to form homogeneous solution. The solution was gradually heated to ~120 °C with

regular stirring until the light green suspension became a paste. The product was oven dried at 80 °C overnight. Finally, the resulting dried samples were ground and calcined at 550 °C (2 °C min^{-1}) under N_2 flow for 1 h followed by air flow for 6 h.

Characterization

All the catalysts were characterized using PHILIPS-binary XPert with MPD Cu Kα diffractometer for wide angle analysis. The analysis was operated at radiation of 30 mA, 40 kV and scanned from 5° to 80° with increasing steps of 0.020°. The characterization of low angle XRD was performed by Bruker type D2 phaser with KFL CuKα radiation at 10 mA, 30 kV and scanned at 2° to 10° in steps of 0.020°. The textural properties were determined using N_2 adsorption–desorption of Quantachrome Touchwin v1.11 instrument. Quantachrome ASiQwin instrument was used to calculate the pore size distribution by NLDFT method. The acidity of the catalysts were determined using pyridine-FTIR (Shimadzu Instrument Spectrum One 8400S). The catalyst was pelleted (15 mg) and placed in tubular glass equipped with CaF_2 window. The samples were heated at 400 °C for 4 h under N_2 flow to remove impurities and cooled to room temperature. The pellet was exposed with pyridine vapour until saturation. The sample was then heated at 150 °C for 3 h to remove the physisorbed pyridine and then analysed using FTIR at 1600–1400 cm^{-1}. High resolution-TEM analysis were carried out using Hitachi HR-9500 TEM with acceleration voltage of 300 kV. The fresh and spent catalysts were characterized using thermogravimetric analysis (TGA) Linseis STA PT-1000. The samples were heated in the range of 28 to 600 °C with heating rate of 10 °C min^{-1} under air flow.

Deoxygenation reaction

Reutealis trisperma oil (RTO) was used as feedstock for the catalytic deoxygenation reaction. The physicochemical properties of RTO were summarized in Table 2. Deoxygenation was carried out using semi-batch reactor equipped with distillation system and mechanically stirred heating mantle. In each catalytic reaction, 3% of catalyst and 10 g of RTO were added in a three-necked flask reactor. Before the reaction, nitrogen gas was used to evacuate the air to ensure the reaction was carried out under inert atmosphere. The mixture was stirred and heated to 350 °C for 4 h. The liquid product was collected for analysis using GC-MS. The reaction was repeated twice to investigate the reproducibility of the results.

Table 2 Physicochemical properties of *Reutealis trisperma* oil

Oil properties	RTO
Density (g cm^{-3})	0.93
Viscosity at 40 °C (cSt)	102.22
Moisture content (wt%)	0.0014
Acid value (mg KOH per g)	4.27
FFA value (%)	0.36

Deoxygenated liquid product analysis

Liquid products from deoxygenation reaction were analysed using gas chromatography-mass spectroscopy (HP 6890 GC). HP-5MS was used as capillary column (length: 30 m × inner diameter: 0.25 mm × film thickness: 0.25 μm). 1-Bromohexane was used as internal standard for quantitative analysis. The peak area from GC-MS analysis were used to calculate the yield of various products and to confirm the components of the liquid products. The degree of deoxygenation was calculated based on the amount of fatty acid (FA) in RTO and liquid product (eqn (1)), while the percentage of liquid yield was determined using eqn (2). The selectivity of hydrocarbon was calculated using eqn (3).

$$\text{Degree of deoxygenation} = \left[1 - \left(\frac{\%\ \text{FA in liquid product}}{\%\ \text{FA in reactant}}\right)\right] \times 100\% \quad (1)$$

$$\text{Liquid yield} = \left(\frac{\text{weight of liquid product}}{\text{weight of reactant}}\right) \times 100\% \quad (2)$$

$$\text{Selectivity} = \frac{(\text{peak area of desired hydrocarbon})}{(\text{peak area of total hydrocarbon})} \times 100\% \quad (3)$$

The selectivity of liquid products, solid char and non-condensable gas were determined based on the percentage of weight as shown in eqn (4)–(6).

$$\text{Liquid selectivity} = \frac{\text{weight of liquid products}}{\text{total weight of liquid, solid char and gas}} \times 100\% \quad (4)$$

$$\text{Solid char selectivity} = \frac{\text{weight of solid char}}{\text{total weight of liquid, solid char and gas}} \times 100\% \quad (5)$$

$$\text{Non-condensable gas selectivity} = \frac{\text{weight of non-condensable gas}}{\text{total weight of liquid, solid char and gas}} \times 100\% \quad (6)$$

Results and discussion

XRD analysis

XRD analysis of Al-MCM-41 and Ni/Al-MCM-41 at different weight loading were shown in Fig. 1. The wide angle diffraction pattern showed the typical amorphous broad peak between 15–30° in all of the catalysts, corresponded to the amorphous phase of the Al-MCM-41 support[39] (Fig. 1a). The presence of NiO was observed at $2\theta = 37.13°$ (111), 43.2° (200), and 62.79° (220), which were ascribed to the face-centered cubic NiO (JCPDS 01-075-0197).[14] The intensity of NiO diffraction peaks were increased at higher Ni loading. The average crystallite sizes of NiO were calculated using Debye–Scherrer method based on the (111)

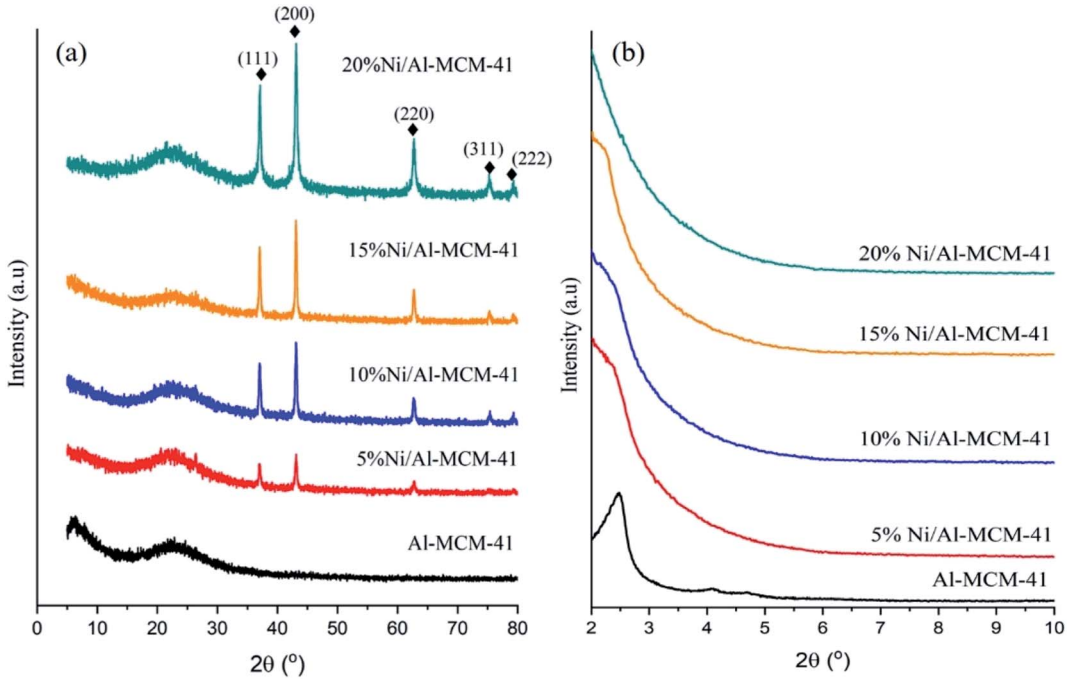

Fig. 1 (a) Wide angle and (b) low angle XRD patterns of the catalysts.

plane and summarized in Table 3. The low angle XRD analysis was used to investigate the effect of NiO impregnation on the ordered hexagonal pore structure of Al-MCM-41 (Fig. 1b). The low angle XRD analysis of Al-MCM-41 showed three diffraction peaks at 2θ: 2.46°; 4.08° and 4.73° which were corresponded to the (100), (110) and (200) diffraction planes, respectively. These peaks confirmed the formation of highly ordered hexagonal mesostructures of Al-MCM-41.[35] Following impregnation with NiO at 5%, the sharp peak of (100) diffraction plane at 2.5° that was associated with a highly ordered hexagonal mesopore was transformed into a broad peak, meanwhile the 4.08° and 4.73° were disappeared. When the NiO loading was further increased to 20%, the low angle peak at 2.5° of Al-MCM-41 was further deteriorated, suggesting the reduction of regularity of mesoporous molecular channel of Al-MCM-41.[40]

N_2 adsorption–desorption analysis

Fig. 2a shows the N_2 adsorption–desorption isotherms of the catalysts and Table 3 summarized the textural properties calculated from the data. All the catalysts exhibited type IV isotherm, which was the typical isotherm for mesoporous material. A gradual increase of the nitrogen uptake between the relative pressures (P/P_0) of 0.25–0.42 was due to the capillary condensation in the uniform mesopore of Al-MCM-41.[41–43] The pore volume and the surface area of Al-MCM-41 were significantly reduced with the increase of NiO loading. Nonetheless, the catalysts still showed the mesoporous feature even after impregnation with 20% NiO. Fig. 2b shows the changes of the pore size distribution after NiO impregnation. The large pore volume of the Al-MCM-41 was due to the presence of intraparticle mesopores at diameter between 3.0–4.5 nm. Increasing the NiO loading to 20% have significantly reduced the pore volume of the catalysts, which implied the possibility of NiO deposition within the mesopores. It is interesting to see that the distribution of the pore size diameter only showed a slight variation following impregnation with NiO, suggesting the impregnation of Ni nanoparticles only caused a partial blockage of the Al-MCM-41 pores.[37]

Table 3 Structural properties of Al-MCM-41 and 5, 10, 15 and 20% Ni/Al-MCM-41

	Surface area ($m^2\ g^{-1}$)			Pore volume ($cc\ g^{-1}$)						Number of acid sites ($mmol\ g^{-1}$)		
Ni (%)	S_{BET}[a]	S_{meso}	S_{micro}[b]	V_{total}	V_{meso}	V_{micro}[b]	D_{meso} (nm)	Ni[c] (%)	NiO size[d] (nm)	Brønsted	Lewis	Lewis density[e] ($\mu mol\ m^{-2}$)
0	739	260	478	0.845	0.559	0.286	3.8	—	—	0.116	0.137	0.185
5	439	247	188	0.584	0.458	0.126	3.60	4.7	23	0.031	0.315	0.717
10	372	224	147	0.529	0.435	0.094	3.55	8.8	26	0.050	0.296	0.796
15	360	208	170	0.519	0.402	0.117	3.53	12.5	27	0.063	0.281	0.780
20	302	144	158	0.318	0.224	0.094	3.29	15.0	26	0.046	0.126	0.417

[a] S_{BET} (surface area) by BET method. [b] S_{micro} and V_{micro} by *t*-plot method. [c] SEM-EDX. [d] Calculated using the Scherrer equation based on the XRD diffraction pattern of (111) plane. [e] Lewis density = Lewis acid sites/S_{BET}.

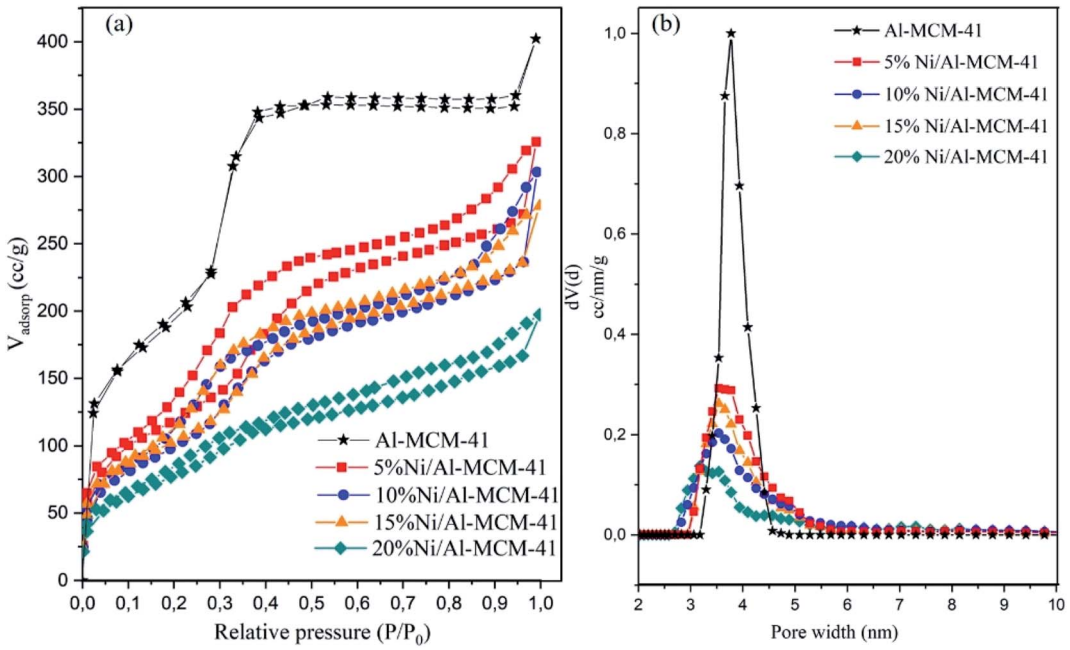

Fig. 2 N_2 adsorption–desorption isotherms (a) and pore size distributions by DFT method (b) of the catalysts.

Pyridine-FTIR analysis

Pyridine was used as a probe molecule for determination of acidity based on the chemical interaction between pyridine with Lewis and Brønsted acid sites (Fig. 3). The absorption band at 1450 cm^{-1} was due to the interaction between the nitrogen atoms in pyridine with the Lewis acid sites in the catalysts. The lone-pair electron of nitrogen in pyridine was co-ordinately bounded with the vacant orbital of the metal oxide which generated the shift of the electron density, thus resulting in a characteristic absorption band of the Lewis acid.[44] Apart from that, the absorption band at 1545 cm^{-1} was assigned to the formation of pyridinium ions with Brønsted acid sites.[45,46] The peak intensity of the Brønsted sites were significantly smaller than the Lewis sites for all the catalysts. The amount of Lewis acid sites were enhanced following impregnation with NiO up to 15% of loading. Lewis acidity was reduced when NiO loading was further increased to 20% (Table 3). Al-MCM-41 was synthesised at the SiO_2/Al_2O_3 molar ratio of 50, resulting in the formation of catalysts with the low amount of acidity. NiO provided the additional Lewis acid in Al-MCM-41. However, at much higher NiO loading, there is a possibility that NiO particles were distributed closely thus reducing the ability of pyridine molecules to interact with the acid sites. The size of NiO determined from Scherrer equation (Table 3) was similar at different weight loadings, approximately 20 nm. However, the fact that the surface area was reduced with increasing NiO loading implied the close proximity between NiO crystallites that occupied the external surface area of Al-MCM-41. Unlike Lewis acidity, the presence of NiO on Al/MCM-41 reduced the amount of Brønsted sites presumably due to the exchange of the proton in the Si–O–Al framework with the Ni^{2+} ion.[47] However, increasing the loading to 20% did not show further reduction of Brønsted acid sites indicating the saturation of the ion exchanged process.[48] Pyridine analysis confirmed the addition of NiO only enhanced the amount of Lewis acidity, thus the changes in the catalytic activity can be correlated with the effect of Lewis acidity rather than Brønsted acidity.

Morphology analysis using FE-SEM and TEM

FE-SEM analysis of Ni/Al-MCM-41 at different weight loading showed the morphology was changed with the increase of NiO loading. At 5% loading, small crystallites with irregular spherical morphology was observed. However at 20% loading, the small crystallites were agglomerated to form larger aggregates (Fig. 4). The EDX mapping was used to analyse the distribution of nickel nanoparticles on Al-MCM-41. At 5% loading, NiO was widely distributed on Al-MCM-41 with a clear separation between the particles. Following impregnation at much higher NiO loading, the NiO nanoparticles became more closely distributed with much shorter distances between the particles. The amount of Ni determined from EDX analysis were in a good agreement with the experimental value (Table 3). 10%Ni/Al-MCM-41 was further characterized using TEM analysis to determine the particle size of NiO (Fig. 5). The TEM results further confirmed the FESEM-EDX analysis that showed a homogeneous dispersion of nickel nanoparticles on Al-MCM-41. The presence of small NiO particles were observed at ~3–4 nm thus can be used to prove the deposition of NiO within the mesopores. Apart from that, NiO also formed a large aggregate at ~22 nm of diameter. The NiO crystallite size was large enough to be deposited into the mesopores of Al-MCM-41, and therefore it is very likely that some of NiO was also impregnated on the external surface of the support. The lattice spacing of Al-MCM-41 was also determined at 3.5 nm.

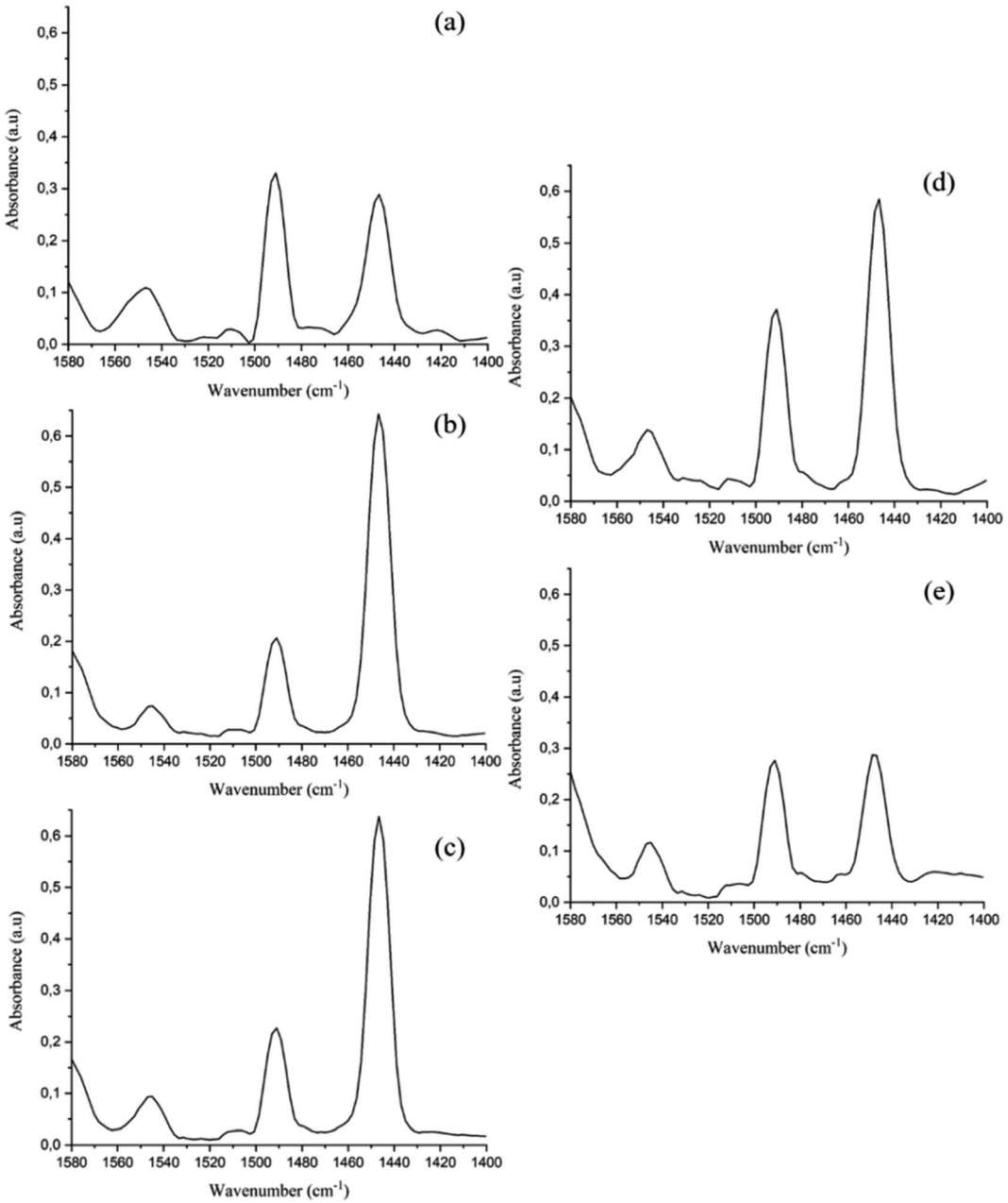

Fig. 3 Pyridine-FTIR analysis of the catalysts after desorption at 150 °C for Al-MCM-41 (a), 5–20% Ni/Al-MCM-41 (b–e).

Catalytic activity of RTO

Deoxygenation of RTO was conducted at 350 °C for 4 h under N_2 flow by using semi-batch flow reactor. In general, products from deoxygenation of RTO were divided into liquid product, non-condensable gas and carbon char (Table 4). Al-MCM-41 showed 51.8% of oil conversion, and from the converted oil only 19.32% were in the form of liquid yield. Following impregnation with 10% NiO, the amount of converted oil was significantly increased to 68.3% and produced 33.2% of liquid yield. However, the conversion was reduced at 20% loading to give 48.0% of conversion. As shown in Table 3, increasing the NiO loading enhanced the number of Lewis acid density. The increase of Lewis acid sites improved the catalytic deoxygenation of RTO, which implied the C–C bond dissociation occurred on Lewis sites. However as the NiO loading was increased to 20%, Lewis acidity was significantly reduced which consequently decreased the conversion of RTO.

The activity of the catalysts were also examined based on the degree of deoxygenation (DO). Liquid product obtained from the reaction was further analysed using GC-MS to obtain the distribution of the deoxygenated compounds. The identified liquid products were tabulated in the ESI (Table S1†). DO was defined as the reduction of fatty acid (FA) concentration in the liquid products relative to the FA content in the RTO oil.[49] DO was significantly increased to 100% following impregnation

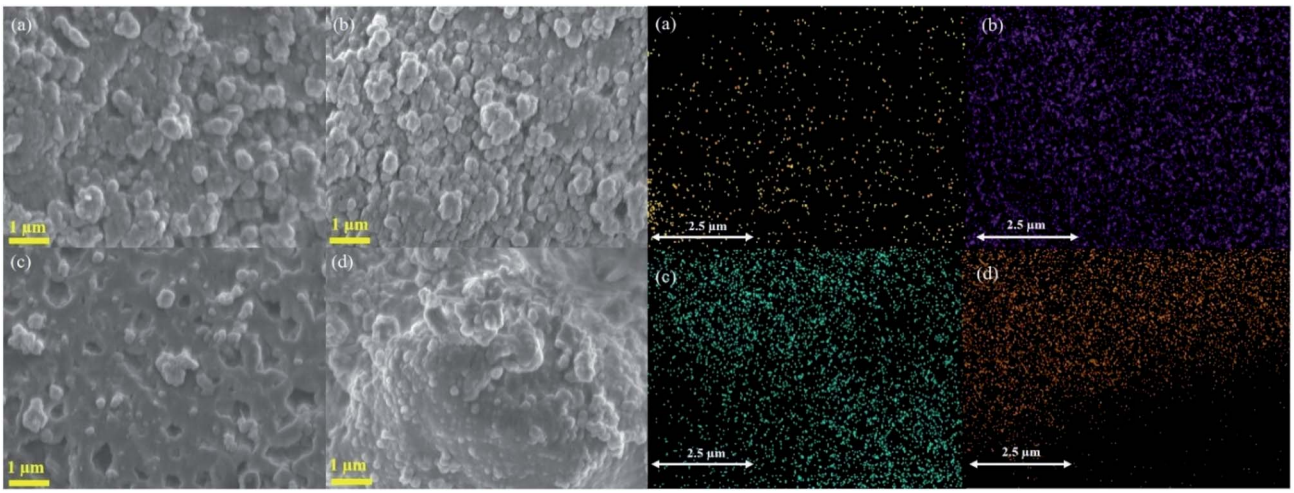

Fig. 4 FESEM-EDX analysis of the 5%Ni/Al-MCM-41 (a), 10%Ni/Al-MCM-41 (b), 15%Ni/Al-MCM-41 (c) and 20%Ni/Al-MCM-41 (d).

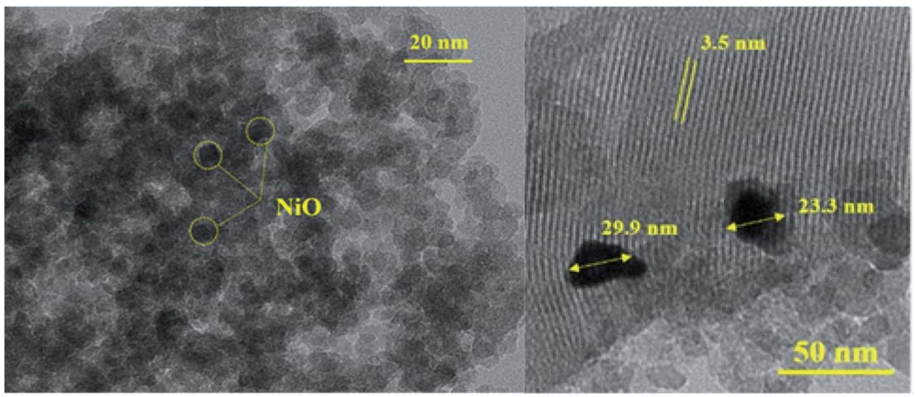

Fig. 5 HR-TEM images of 10%Ni/Al-MCM-41.

Table 4 Deoxygenation of RTO at 350 °C for 4 h under N_2 flow using Al-MCM-41 catalysts at different NiO loading

NiO (%)	Conversion (%)	$Sel._{liquid}$ (%)	$Sel._{gas}$ (%)	$Sel._{char}$ (%)	Liquid yield (%)	DO (%)
0	51.8	35.11	61.98	2.90	19.32	95.2
5	57.5	40.77	55.56	3.66	25.32	96.9
10	68.3	43.61	51.39	4.98	33.20	100.0
15	60.0	49.47	46.35	4.17	32.41	99.8
20	48.0	43.81	53.18	2.99	22.39	98.0

with NiO at 10% loading. The amount of the oxygenated compounds such as alcohol, ketone and aldehyde were reduced meanwhile negligible amount of carboxylic acid were analysed from the liquid product. Ideally, in the deoxygenation reaction, the catalysts should remove the oxygenated carbon in FA while inhibiting the hydrocracking reaction in order to maintain the long chain hydrocarbon structures. As shown in Fig. 6a, the composition of liquid products were dominated by the hydrocarbon molecules, however compounds such as aromatic, cyclic, aldehyde and ketone were also identified at a very low concentration. In the absence of Ni, the amount of carboxylic acid was analysed on Al-MCM-41 at ~9%, suggesting the inefficiency of deoxygenation reaction. Increasing the NiO loading to 10% enhanced the hydrocarbon yield while significantly reduced the amount of carboxylic acid and the other oxygenates compounds. The results highlighted the role of NiO to enhance Lewis acidity in order to ensure the efficient deoxygenation reaction of RTO.

GCMS analysis of the liquid product showed the production of hydrocarbon biofuels within the diesel range *i.e.* C11–18 (Fig. 6b). The GCMS spectra of deoxygenated liquid product using 10%Ni/Al-MCM-41 catalyst were shown in Fig. S1 in ESI.† The C11–18 hydrocarbon yield increased with the increase of NiO loading up to 10%. The RTO used in this reaction consisted of palmitic acid (C16:0), oleic acid (C18:1) and linoleic acid (C18:0) as summarized in Table 5. In principle, the deoxygenation reaction eliminated the carboxylic and/or the carbonyl fragments from the fatty acid to form straight-chain hydrocarbons *via* the decarboxylation-/decarbonylation reaction (deCOx).[50] The majority of hydrocarbons from the catalytic

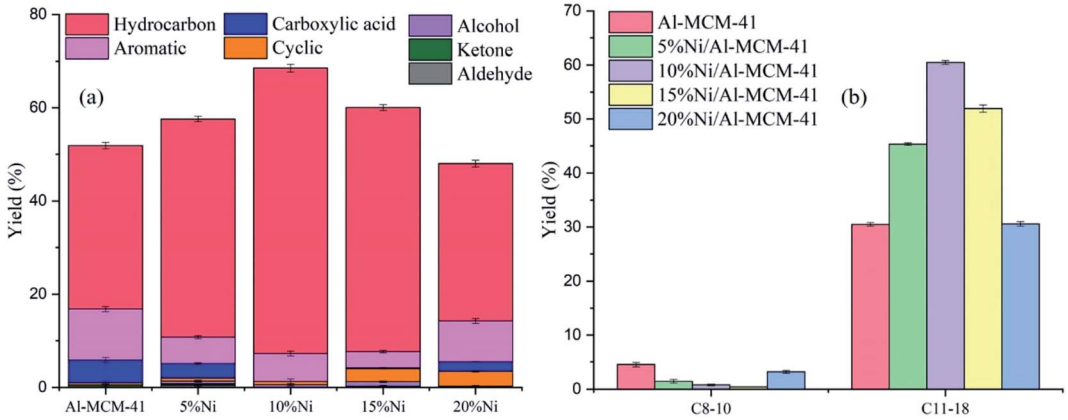

Fig. 6 (a) Distribution of liquid products and (b) distribution of hydrocarbon from catalytic deoxygenation of RTO; gasoline (C8–10) and diesel (C11–18).

Table 5 Composition of RTO as carbon feedstock and the biofuels obtained from deoxygenation using Al-MCM-41 and 10%Ni/Al-MCM-41 catalysts

	RTO		Al-MCM-41		10%Ni/Al-MCM-41	
Carbon number	C–C, %	C=C/C≡C, %	C–C, %	C=C/C≡C, %	C–C, %	C=C/C≡C, %
8	—	—	0.30	—	—	—
9	—	—	1.03	0.52	—	—
10	—	—	1.80	0.89	0.80	—
11	—	—	2.46	—	1.30	—
12	—	—	3.25	2.22	1.66	—
13	—	—	5.56	1.00	2.89	—
14	—	—	4.52	—	4.20	—
15	—	—	8.83	—	14.36	0.58
16	40.35	—	0.47	—	3.96	0.84
17	3.39	—	2.19	—	28.69	2.01
18	11.84	44.42	—	—	—	—
Total	55.58	44.42	30.41	4.63	57.86	3.43
Selectivity (%)			86.77	13.23	94.40	5.60

deoxygenation of RTO using 10%Ni/Al-MCM-41 were identified as C15 and C17. However, when Al-MCM-41 was used as catalyst, the hydrocarbons were analysed as C8–17 having a similar distribution (Table 5). Following impregnation with NiO, hydrocarbons with one atom carbon shorter than the parent fatty acids produced, suggesting that the decarboxylation is the main catalytic reaction on Ni/Al-MCM-41 catalysts that occurs. However in the absence of NiO, secondary cracking reaction occur resulting in the formation of short chain hydrocarbon (C8–10). Catalysts with a high density of Brønsted acid sites were reported to form strong interaction with olefins enhancing the lifetime of the carbenium ion, therefore resulting in the formation of cracking products.[51] When the Al-MCM-41 was impregnated with NiO, it is clear that Brønsted acidity was reduced meanwhile Lewis acidity was significantly increased. Lewis acidity showed a greater ability to abstract hydride ion than Brønsted acidity[51] in order to react with the chemisorbed oxygen on the catalysts.[52] Therefore the course of the reaction was changed from catalytic cracking in Al-MCM-41 to undergo the deoxygenation route in Ni/Al-MCM-41 (Scheme 1). Most of the hydrocarbons analysed in the biofuels when using NiO/Al-MCM-41 as catalysts were C17:0 (28.7%) and C15:0 (14.36%), which can be identified as the products from deoxygenation of C18:0 and C16:0 triglycerides in the RTO.

Apart from carbon number, the hydrocarbons can be divided further into the saturated (C–C) and the unsaturated (C=C/C≡C) molecules. The composition of biofuels summarized in Table 5 showed the majority of the hydrocarbons produced when using Al-MCM-41 and 10%Ni/Al-MCM-41 catalysts were saturated molecules at ~86–94% selectivity. The unsaturated molecules in the biofuels were analysed at ~3–4%, which was significantly lower than the composition of the unsaturated molecules in RTO which was at ~44.42%. There is also a possibility that the unsaturated triglyceride in RTO underwent cracking reaction to form smaller hydrocarbons or non-condensable gases. It is understood that olefin was more susceptible towards cracking reaction than paraffin, thus reducing the composition of the unsaturated hydrocarbon in the biofuels.[53]

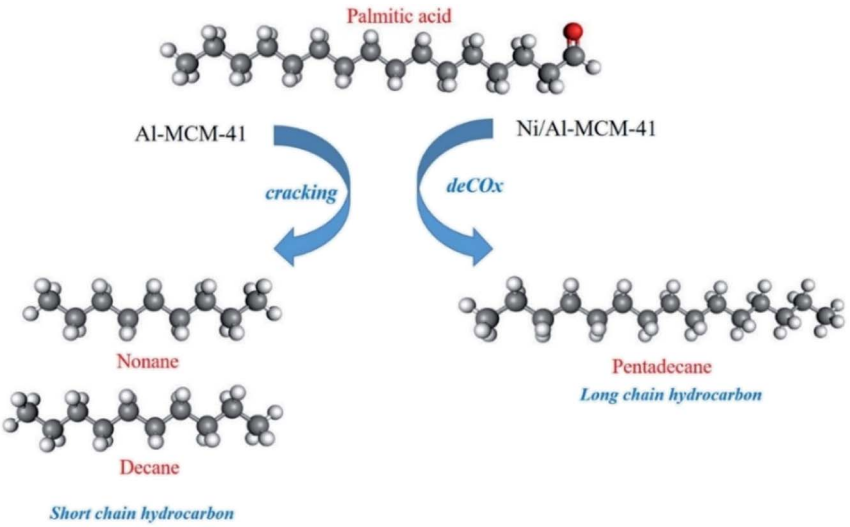

Scheme 1 Catalytic transformation of RTO to biofuels on Al-MCM-41 and Ni/Al-MCM-41 catalysts.

Reusability of 10%Ni/Al-MCM-41 catalyst

The reusability studies were carried out using 10%Ni/Al-MCM-41 in order to determine the stability of the catalyst. The catalyst was filtered after 4 h of reaction and washed with hexane in order to remove the residual reactant/product. The catalyst was reused under similar reaction condition for up to four reaction cycles. Fig. 7a showed the conversion was slightly reduced to 55% at the second reaction cycle and 50% after the fourth cycle. The liquid yield was also reduced from 33% to 19% after four consecutive reactions. Analysis of the liquid product indicated the selectivity of hydrocarbon was reduced from 89% to 54% after the second reaction cycle (Fig. 7b). The amount of carboxylic acid product was enhanced when the catalyst was used repeatedly which implied the inefficiency of the catalyst to drive deoxygenation reaction. The loss of active sites is likely due to the formation of carbon coke or the sintering of metal particle deactivating the catalyst.[37]

Analysis of coke – TG-DTA analysis

In general, heterogeneous acid catalysts experienced carbon deposition on the surface during deoxygenation that can lead to deactivation. Acid catalyst is crucial for C–C bond dissociation, however it can also initiate coke formation.[18] TGA analysis of the fresh 10%Ni/Al-MCM-41, spent Al-MCM-41 and spent 10% Ni/Al-MCM-41 catalysts under air were carried out to determine the amount of coke (Fig. 8). The 10%Ni/Al-MCM-41 catalyst was stable up to 600 °C, however 15.15% of total weight loss measured occurred below 100 °C indicating the removal of physisorbed water. Analysis of Al-MCM-41 and 10%Ni/Al-MCM-41 recovered after deoxygenation showed a total weight loss of 25% and 43% respectively. The continuous weight loss up to 600 °C was due to the oxidation of carbonaceous coke on the spent catalysts to CO_2.[54] The feature was accompanied with the DTA profiles indicating the endothermic process of carbon oxidation. For 10%Ni/Al-MCM-41 catalyst, two DTA peaks were

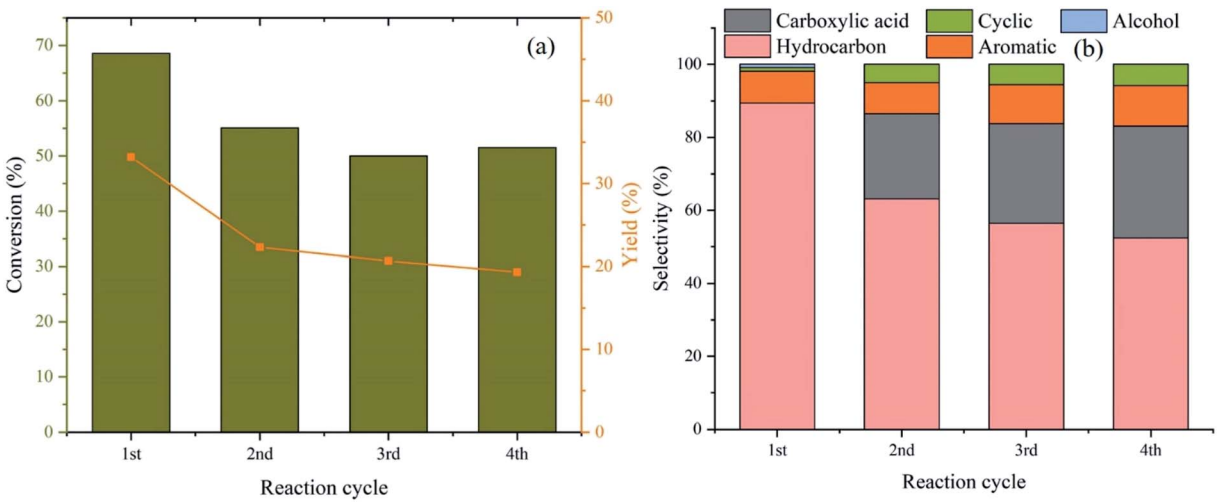

Fig. 7 Conversion and liquid yield from deoxygenation of RTO after 4 reaction cycles (a), and distribution of liquid product (b). 10%Ni/Al-MCM-41 was used as the catalysts.

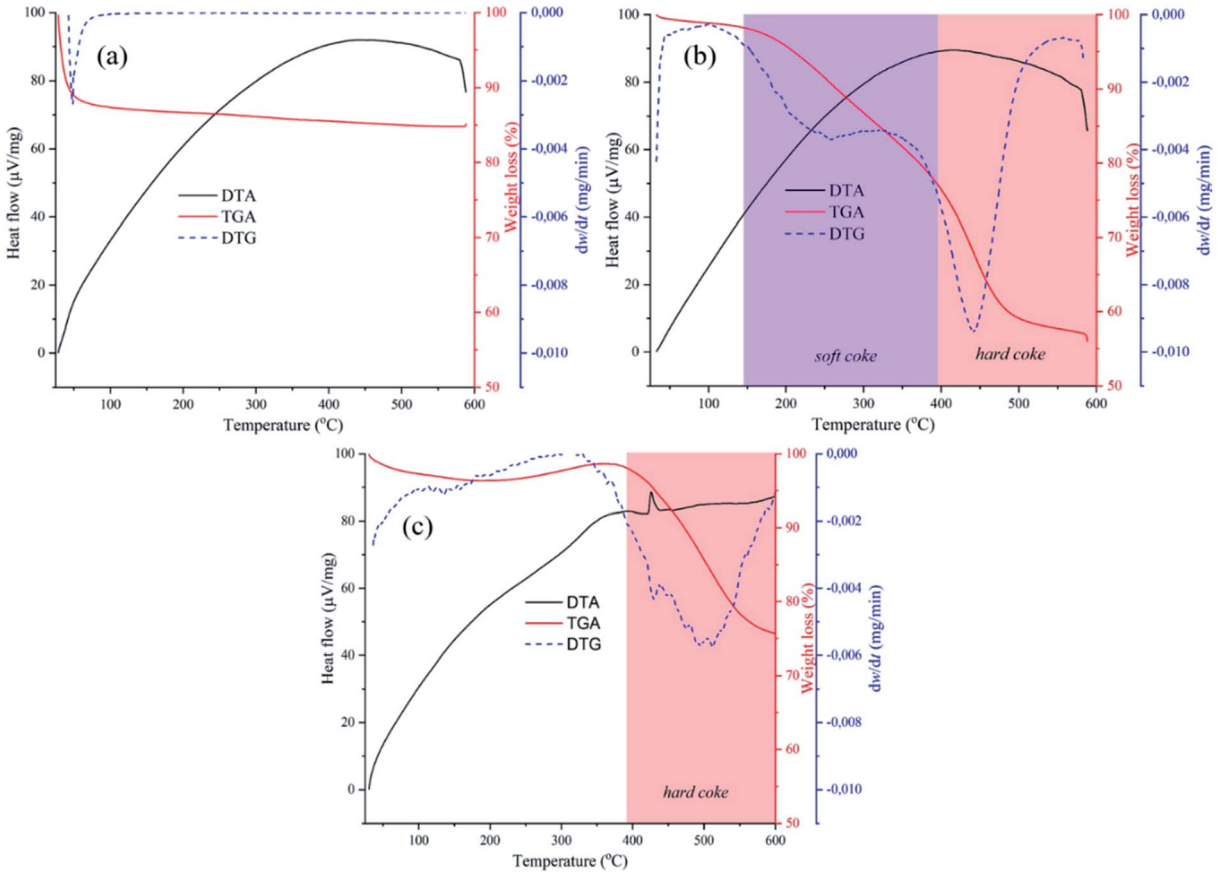

Fig. 8 TG-DTG-DTA profile of (a) 10%Ni/Al-MCM-41 fresh, (b) 10%Ni/Al-MCM-41 spent and (c) Al-MCM-41 spent catalysts.

observed at temperature below 500 °C which corresponded to decomposition of soft or thermal cokes. The soft coke consisted of aliphatic hydrocarbon which was in agreement with the major product analysed from 10% Ni loading. In spent Al-MCM-41 catalyst, the combustion of coke occurred at much higher temperatures ~400–600 °C suggesting the formation of hard

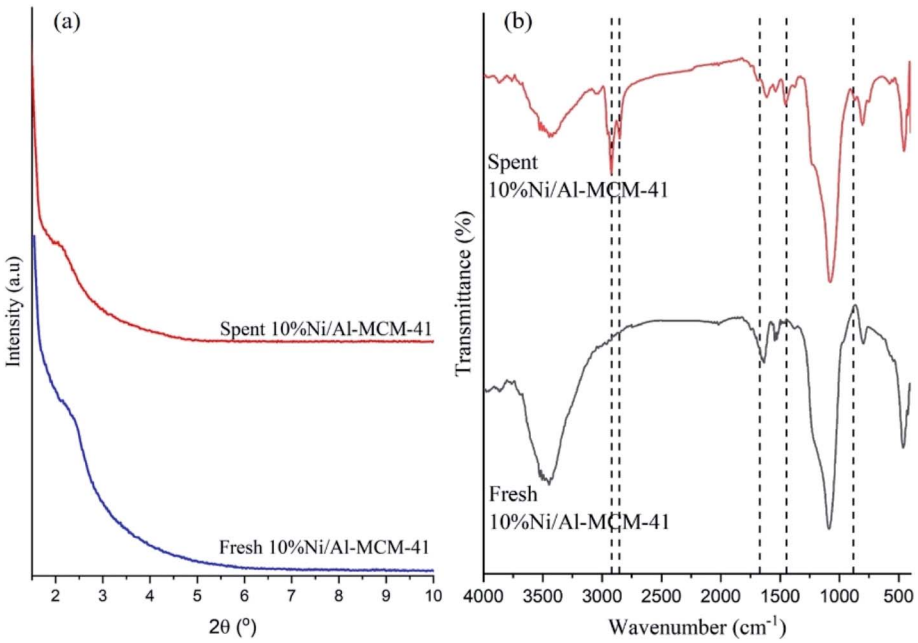

Fig. 9 Low angle XRD pattern (a) and FTIR spectra (b) of fresh and spent 10%Ni/Al-MCM-41 catalyst.

coke such as polyaromatic carbon that required oxidation at high temperatures.[11,55,56] The derivative thermal analysis (DTA) of the spent Al-MCM-41 showed a broad exothermic peak that corresponded to the decomposition of coke consisting of aromatics carbon residue which was also the second major component of the liquid product. It is interesting to note that the results from TGA analysis confirm that the presence of NiO reduces the formation of aromatic compound thus reducing the deposition of hard coke from aromatic carbon on the catalyst during deoxygenation reaction.

Low angle XRD and FTIR analysis of spent catalyst

XRD analysis of 10%Ni/Al-MCM-41 catalysts before and after catalytic reaction in Fig. 9a showed the intensity of (100) diffraction plane at $2\theta = 2.3$ was reduced after reaction suggesting the deposition of carbon coke in the hexagonal pores of Al-MCM-41. The presence of coke within the pores reduced the accessibility and the diffusion of the reactant to reach the active sites.[36] The catalysts were further characterised using FTIR analysis (Fig. 9b) in order to identify the nature of carbon coke that was formed on the spent catalyst. The specific region for characterization of coke is between 1300–1700 cm^{-1} and 2800–3100 cm^{-1}.[57–59] The absorption peak at 3449 cm^{-1} that was attributed to the associated OH group showed significant reduction in intensity after reaction. The new absorption bands at 2866 cm^{-1} and 2910 cm^{-1} were observed on the spent catalyst which were ascribed to the symmetric and the asymmetric stretching vibration of C–H in CH_3 and CH_2 aliphatic carbon.[60,61] The vibration bands at 1380–1680 cm^{-1} were assigned to the stretching vibration of C=C in poly condensed aromatic rings and CH_3 bending of paraffinic residue.[57] The results obtained from FTIR analysis further confirmed the formation of aromatic and aliphatic coke deposited on the catalysts during the deoxygenation reaction.

Conclusion

Catalytic deoxygenation of *Reutealis trisperma* oil under H_2-free condition was investigated using Lewis acid Ni/Al-MCM-41 catalysts. Nickel enhanced the activity Al-MCM-41 to give high conversion and high selectivity toward hydrocarbons within the diesel range. Impregnation of NiO on mesoporous Al-MCM-41 only showed the increase of Lewis acidity but not Brønsted acidity. Detail analysis of the distribution of hydrocarbon indicated that the C11–18 hydrocarbon yield were increased following NiO impregnation up to 10% loading. The formation of C15 and C17 hydrocarbon molecules suggested the efficiency of Ni/Al-MCM-41 catalysts to drive the course of catalytic reaction towards deoxygenation pathway. In the absence of Ni, Al-MCM-41 showed the formation of short chain hydrocarbon as the result of cracking reaction. The presence of NiO enhanced the catalytic conversion of RTO into green diesel hydrocarbon *via* decarboxylation–decarbonylation routes due to the increased of Lewis acidity.

Author contributions

Reva Edra Nugraha: conceptualization, methodology, investigation, validation, writing – original draft. Didik Prasetyoko: conceptualization, methodology, validation, supervision, writing – review & editing, resources. Hasliza Bahruji: supervision, validation, writing – review & editing. Suprapto Suprapto: supervision, validation. Nurul Asikin-Mijan: investigation, validation, writing – review & editing. Titie Prapti Oetami: resources. Aishah Abdul Jalil: validation, conceptualization, resources. Dai-Viet N. Vo: validation, conceptualization. Yun Hin Taufiq-Yap: supervision, resources.

Conflicts of interest

There are no conflicts to declare.

Acknowledgements

The authors would like to acknowledge the Ministry of Research, Technology and Higher Education of Republic Indonesia for the financial support under PMDSU scholarship with contract number 1290/PKS/ITS/2020 and basic research grant with contract number 778/PKS/ITS/2021.

Notes and references

1 K. Kusmiyati, D. Prasetyoko, S. Murwani, M. N. Fadhilah, T. P. Oetami, H. Hadiyanto, W. Widayat, A. Budiman and A. Roesyadi, *Energies*, 2019, **12**, 2–11.
2 W. N. Adira Wan Khalit, T. S. Marliza, N. Asikin-Mijan, M. S. Gamal, M. I. Saiman, M. L. Ibrahim and Y. H. Taufiq-Yap, *RSC Adv.*, 2020, **10**, 37218–37232.
3 P. Balakrishnan, M. S. Shabbir, A. F. Siddiqi and X. Wang, *Energy Sources, Part A*, 2020, **42**, 2698–2703.
4 T. Prasomsri, W. Jiao, S. Z. Weng and J. Garcia Martinez, *Chem. Commun.*, 2015, **51**, 8900–8911.
5 B. P. Pattanaik and R. D. Misra, *Renewable Sustainable Energy Rev.*, 2017, **73**, 545–557.
6 G. J. S. Dawes, E. L. Scott, J. Le Nôtre, J. P. M. Sanders and J. H. Bitter, *Green Chem.*, 2015, **17**, 3231–3250.
7 M. Choo, L. E. Oi, T. C. Ling, E. Ng, Y. Lin, G. Centi and J. C. Juan, *J. Anal. Appl. Pyrolysis*, 2020, 104797.
8 M. Li, S. Xing, L. Yang, J. Fu, P. Lv, Z. Wang and Z. Yuan, *Appl. Catal., A*, 2019, **587**, 117112.
9 C. Hu, X. Du, D. Li, H. Xin, W. Zhou, R. Yang and K. Zhou, *Energy Technol.*, 2019, **7**, 1–14.
10 N. Asikin-Mijan, H. V Lee, G. Abdulkareem-Alsultan and A. Afandi, *J. Cleaner Prod.*, 2017, **167**, 1048–1059.
11 N. Asikin-Mijan, J. M. Ooi, G. AbdulKareem-Alsultan, H. V. Lee, M. S. Mastuli, N. Mansir, F. A. Alharthi, A. A. Alghamdi and Y. H. Taufiq-Yap, *J. Cleaner Prod.*, 2020, **249**, 119381.
12 A. Yıldız, J. L. Goldfarb and S. Ceylan, *Fuel*, 2019, 1–7.
13 G. Abdulkareem-Alsultan, N. Asikin-Mijan, N. Mansir, H. V. Lee, Z. Zainal, A. Islam and Y. H. Taufiq-Yap, *J. Anal. Appl. Pyrolysis*, 2019, **137**, 171–184.

14 K. B. Baharudin, Y. H. Taufiq-Yap, J. Hunns, M. Isaacs, K. Wilson and D. Derawi, *Microporous Mesoporous Mater.*, 2019, **276**, 13–22.
15 M. S. Gamal, N. Asikin-Mijan, W. N. A. W. Khalit, M. Arumugam, S. M. Izham and Y. H. Taufiq-Yap, *Fuel Process. Technol.*, 2020, **208**, 106519.
16 J. de Barros Dias Moreira, D. Bastos de Rezende and V. Márcia Duarte Pasa, *Fuel*, 2020, **269**, 117253.
17 H. Hartati, W. Trisunaryanti, R. R. Mukti, I. A. Kartika, P. B. Dea Firda, S. D. Sumbogo, D. Prasetyoko and H. Bahruji, *J. Energy Inst.*, 2020, **93**, 2238–2246.
18 Y. L. Tan, A. Z. Abdullah and B. H. Hameed, *Fuel*, 2019, **245**, 89–95.
19 T. M. I. Riayatsyah, H. C. Ong, W. T. Chong, L. Aditya, H. Hermansyah and T. M. I. Mahlia, *Energies*, 2017, **10**, 1–21.
20 H. Holilah, D. Prasetyoko, T. P. Oetami, E. B. Santosa, Y. M. Zein, H. Bahruji, H. Fansuri, R. Ediati and J. Juwari, *Biomass Convers. Biorefin.*, 2014, **5**, 347–353.
21 S. Suprapto, T. R. Fauziah, M. S. Sangi, T. P. Oetami, I. Qoniah and D. Prasetyoko, *Indones. J. Chem.*, 2016, **16**, 208–213.
22 A. S. Silitonga, T. M. I. Mahlia, F. Kusumo, S. Dharma, A. H. Sebayang, R. W. Sembiring and A. H. Shamsuddin, *Renewable Energy*, 2019, **133**, 520–527.
23 A. S. Silitonga, T. M. I. Mahlia, H. C. Ong, T. M. I. Riayatsyah, F. Kusumo, H. Ibrahim, S. Dharma and D. Gumilang, *Energy Sources, Part A*, 2017, **39**, 2006–2014.
24 L. Yang, S. Xing, H. Sun, C. Miao, M. Li, P. Lv, Z. Wang and Z. Yuan, *Fuel Process. Technol.*, 2019, **187**, 52–62.
25 M. Li, J. Fu, S. Xing, L. Yang, X. Zhang, P. Lv, Z. Wang and Z. Yuan, *Appl. Catal., B*, 2020, **260**, 118114.
26 N. Aliana-Nasharuddin, N. Asikin-Mijan, G. Abdulkareem-Alsultan, M. I. Saiman, F. A. Alharthi, A. A. Alghamdi and Y. H. Taufiq-Yap, *RSC Adv.*, 2019, **10**, 626–642.
27 J. M. Gómez, E. Díez and I. Bernabé, *Catal. Commun.*, 2016, **78**, 55–58.
28 M. Y. Choo, J. C. Juan, L. E. Oi, T. C. Ling, E. P. Ng, A. Rahman Noorsaadah, G. Centi and K. T. Lee, *Catal. Sci. Technol.*, 2019, **9**, 772–782.
29 E. W. Qian, N. Chen and S. Gong, *J. Mol. Catal. A: Chem.*, 2014, **387**, 76–85.
30 S. Karnjanakom, T. Suriya-umporn, A. Bayu, S. Kongparakul, C. Samart, C. Fushimi, A. Abudula and G. Guan, *Energy Convers. Manage.*, 2017, **142**, 272–285.
31 S. Zulkepli, J. C. Juan, H. V. Lee, N. S. A. Rahman, P. L. Show and E. P. Ng, *Energy Convers. Manage.*, 2018, **165**, 495–508.
32 L. E. Oi, M. Y. Choo, H. V. Lee, Y. H. Taufiq-Yap, C. K. Cheng and J. C. Juan, *Int. J. Hydrogen Energy*, 2020, **45**, 11605–11614.
33 N. Asikin-Mijan, H. V. Lee, J. C. Juan, A. R. Noorsaadah, H. C. Ong, S. M. Razali and Y. H. Taufiq-Yap, *Appl. Catal., A*, 2018, **552**, 38–48.
34 A. Veses, B. Puértolas, J. M. López, M. S. Callén, B. Solsona and T. García, *ACS Sustainable Chem. Eng.*, 2016, **4**, 1653–1660.
35 R. E. Nugraha, D. Prasetyoko, N. Asikin-Mijan, H. Bahruji, S. Suprapto, Y. H. Taufiq-Yap and A. A. Jalil, *Microporous Mesoporous Mater.*, 2021, **315**, 110917.
36 X. Y. Ooi, L. E. Oi, M. Y. Choo, H. C. Ong, H. V. Lee, P. L. Show, Y. C. Lin and J. C. Juan, *Fuel Process. Technol.*, 2019, **194**, 106120.
37 M. F. Kamaruzaman, Y. H. Taufiq-Yap and D. Derawi, *Biomass Bioenergy*, 2020, **134**, 105476.
38 T. Hengsawad, T. Jindarat, D. E. Resasco and S. Jongpatiwut, *Appl. Catal., A*, 2018, **566**, 74–86.
39 N. T. T. Tran, Y. Uemura, S. Chowdhury and A. Ramli, *Appl. Catal., A*, 2016, **512**, 93–100.
40 Z. Jun Wang, Y. Liu, P. Shi, C. Jun Liu and Y. Liu, *Appl. Catal., B*, 2009, **90**, 570–577.
41 N. Cakiryilmaz, H. Arbag, N. Oktar, G. Dogu and T. Dogu, *Catal. Today*, 2019, **323**, 191–199.
42 A. Jafarzadeh, S. Sohrabnezhad, M. A. Zanjanchi and M. Arvand, *J. Solid State Chem.*, 2016, **242**, 236–242.
43 C. Du and H. Yang, *J. Colloid Interface Sci.*, 2012, **369**, 216–222.
44 H. Y. Luo, J. D. Lewis and Y. Román-Leshkov, *Annu. Rev. Chem. Biomol. Eng.*, 2016, **7**, 663–692.
45 H. Li, Y. Wang, F. Meng, H. Chen, C. Sun and S. Wang, *RSC Adv.*, 2016, **6**, 99129–99138.
46 X. Li, D. Han, H. Wang, G. Liu, B. Wang, Z. Li and J. Wu, *Fuel*, 2015, **144**, 9–14.
47 S. Moussa, P. Concepción, M. A. Arribas and A. Martínez, *Appl. Catal., A*, 2020, **608**, 117831.
48 A. Martínez, M. A. Arribas, P. Concepción and S. Moussa, *Appl. Catal., A*, 2013, **467**, 509–518.
49 D. Kubička, J. Horáček, M. Setnička, R. Bulánek, A. Zukal and I. Kubičková, *Appl. Catal., B*, 2014, **145**, 101–107.
50 G. A. Alsultan, N. Asikin-Mijan, H. V. Lee, A. S. Albazzaz and Y. H. Taufiq-Yap, *Energy Convers. Manage.*, 2017, **151**, 311–323.
51 B. Wang, C. Han, Q. Zhang, C. Li, C. Yang and H. Shan, *Energy Fuels*, 2015, **29**, 5701–5713.
52 H. Wang, H. Lin, Y. Zheng, S. Ng, H. Brown and Y. Xia, *Catal. Today*, 2019, **319**, 164–171.
53 J. Abbot and B. W. Wojciechowski, *J. Catal.*, 1989, **115**, 1–15.
54 J. M. Crawford, C. S. Smoljan, J. Lucero and M. A. Carreon, *Catalysts*, 2019, **9**, 1–15.
55 T. Ma, Z. Yun, W. Xu, L. Chen, L. Li, J. Ding and R. Shao, *Chem. Eng. J.*, 2016, **294**, 343–352.
56 T. Techopittayakul, S. Echaroj, M. Santikunaporn, C. Asavatesanupap, Y. H. Chen and M. H. Yuan, *React. Kinet., Mech. Catal.*, 2019, **126**, 529–546.
57 S. Aghamohammadi, M. Haghighi and A. Ebrahimi, *Microporous Mesoporous Mater.*, 2019, **279**, 371–386.
58 H. Zhang, S. Shao, R. Xiao, D. Shen and J. Zeng, *Energy Fuels*, 2014, **28**, 52–57.
59 Y. Li, C. Zhang, Y. Liu, X. Hou, R. Zhang and X. Tang, *Energy Fuels*, 2015, **29**, 1722–1728.
60 Á. Ibarra, A. Veloso, J. Bilbao, J. M. Arandes and P. Castaño, *Appl. Catal., B*, 2016, **182**, 336–346.
61 X. Guo, Y. Zheng, B. Zhang and J. Chen, *Biomass Bioenergy*, 2009, **33**, 1469–1473.